Boundary-Layer Meteorol (2009) 132:193–204
DOI 10.1007/s10546-009-9399-x

ARTICLE

Turbulent Kinetic Energy Dissipation in the Surface Layer

D. Charuchittipan · J. D. Wilson

Received: 20 January 2009 / Accepted: 2 June 2009 / Published online: 19 June 2009

Abstract We estimated the turbulent kinetic energy (TKE) dissipation rate (ϵ) for thirty-two 1-h intervals of unstable stratification covering the stability range $0.12 \leq -z/L \leq 43$ (z/L is the ratio of instrument height to the Obukhov length), by fitting Kolmogorov's inertial subrange spectrum to streamwise spectra observed over a desert flat. Estimated values are compatible with the existence of local equilibrium, in that the TKE dissipation rate approximately equalled the sum of shear and buoyant production rates. Only in the neutral limit was the turbulent transport term in the TKE budget measured to be small.

Keywords Constant stress layer · Dissipation rate · Equilibrium layer · Local equilibrium · Turbulent kinetic energy budget · Turbulent transport · Velocity spectrum · Wall shear layer

1 Introduction

In the context of turbulence closure schemes, it is common to fix coefficients by invoking (along with other idealizations) the assumption that the turbulent kinetic energy (TKE) budget of the adiabatic wall shear layer—and/or the inertial sublayer of the neutral atmospheric surface layer—is in local equilibrium (e.g. "one equation closures," Bradshaw et al. 1967; "two-equation closures," Launder and Spalding 1974; and "Reynolds stress closures," Hanjalic and Launder 1972; Wyngaard et al. 1974). The proposition of local equilibrium, i.e. an exact balance of local TKE production[1] and viscous dissipation (ϵ), emerged from early studies of the turbulent shear layer over a smooth wall, and was held to be plausible in respect of a shallow "equilibrium layer" lying above the viscous wall region[2] (Townsend

[1] In the absence of buoyancy forces, TKE "production" is entirely due to the conversion of mean kinetic energy (MKE), the process generally termed "shear production" and interpreted as "work done by the eddy stresses upon the corresponding rates of mean strain" (Richardson 1920).
[2] By definition, within the 'viscous wall region' the viscous contribution to total shear stress is not negligible (Pope 2000).

D. Charuchittipan · J. D. Wilson (✉)
Department of Earth and Atmospheric Sciences, University of Alberta, Edmonton , AB T6G 2E3, Canada
e-mail: jaydee.uu@ualberta.ca

1961, 1976; Raupach et al. 1991). Cognizant that "the turbulent kinetic energy at a point may depend as much on transport processes from remote parts of the flow as on local production and dissipation," Townsend (1961) nevertheless suggested that in the fully turbulent region of the constant stress layer of a zero-pressure gradient wall shear layer "the basic requirements of energy equilibrium and universality of structure are nearly satisfied." Later Townsend (1976) stated "In general, all terms in the (turbulent kinetic) energy equation are of comparable magnitude but, in some circumstances, only two of them may be significant. The most important case is wall turbulence. Near a rigid boundary, advection and diffusion of energy are both negligible, and (the TKE equation) takes the form (of a balance of shear production and dissipation)."

Perhaps there was a subsequent tendency to omit or underplay the qualifiers ("nearly" and "in general" and "may be")—a survey of literature and textbooks of that epoch amply justifies a remark by Raupach et al. (1991), to the effect that the notion of a local equilibrium prevailing in the wall shear layer became embedded as a sort of folklore. More reserved or nuanced opinions, however, were there to be noted. Tennekes and Lumley (1972) wrote that "in most shear flows production and dissipation do not balance though they are nearly always of the same order of magnitude." Similarly Bradshaw (1978), defining the meaning of local equilibrium in the context of the "thin shear layer approximation," clearly treated it as an *assumption* or *paradigm*, rather than as a concrete fact—and earlier Bradshaw (1967) had stated "production is *roughly* equal to dissipation in all parts of the three boundary layers[3] except the outer edge" (present authors' italics).

Turning specifically to the atmospheric surface layer (ASL), Wyngaard and Coté (1971), reporting the TKE budget as observed in the Kansas experiment, presupposed local equilibrium to hold in the neutral limit, and extrapolating data from non-neutral cases ($-2 \leq z/L$) suggested

$$\phi_\epsilon \left(\frac{z}{L}\right) \equiv \frac{k_v z \epsilon}{u_*^3} = \left(1 + 0.5\,|z/L|^{2/3}\right)^{3/2} \tag{1}$$

(here k_v is the von Karman constant and u_* the friction velocity; later Kaimal (1978) and Caughey and Wyngaard (1979) revised the coefficient multiplying $|z/L|$ from 0.5 to 0.75). This and later experimental evidence regarding the TKE budget of the ASL was incisively reviewed by Frenzen and Vogel (1992), but subsequent careful work by those authors and many others (summarized recently by Li et al. 2008, Table 2) has not made possible a statement (in regard to the presence or absence of local equilibrium) any more universal in scope than that of Tennekes and Lumley. In short, evidence from different field campaigns is not consistent, and some experimenters report that the TKE budget is not in local equilibrium, even in the neutral limit. One common thread of the recent efforts, it is perhaps fair to say, is an implicitly shared view that: (i) the normalized TKE budget, over a suitable height range at a suitable site, *should* be universal under Monin–Obukhov scaling; and, (ii) a discrepancy of some twenty to thirty percent between the (neutral) rates of production and dissipation is worth worrying about[4] and ought to be amenable to resolution. However (i) is probably

[3] Each of the flows referred to was a smooth wall, turbulent, wall shear layer; the three cases were distinguished by the magnitude of the imposed pressure gradient.

[4] On first sight, definitive experimental contradiction of local equilibrium would appear to forbid retention of this paradigm, so convenient in turbulence closure models. However, in actuality, perhaps it barely matters if the paradigm is not literally true to the last percent, provided the closed set of equations is contrived to reproduce the more basic measurable elements of neutral, undisturbed flow, viz. its profiles of mean wind speed, shear stress and TKE.

incorrect, since it has long been known that horizontal velocity statistics do not obey MO scaling; and (ii) may be unduly optimistic, given the many sources of error and uncertainty that surround such, one might say, arcane properties of atmospheric data.

Here we will provide new observations supporting the existence of local equilibrium (at least as a first approximation) over the entire range $0 \leq -z/L \leq 43$. The approach and methods we have used are (by now) entirely conventional, and unlike some earlier authors we have not taken elaborate pains to independently re-evaluate crucial constants (notably the von Karman constant k_v and the Kolmogorov constant α_u defined below). Only an excellent desert site (fetch of many tens of kilometres), its smoothness, and the availability of a pool of modern sonic anemometers distinguish this study from earlier work. The large z/L range sampled is a consequence of small magnitudes of L, due to the smoothness of the desert surface ($z_0 = 0.2$–0.5 mm; Metzger and Holmes 2008) and correspondingly small values of the ratio $u_*/\overline{u}$, i.e. friction velocity to mean wind speed.

2 Methodology

2.1 Site, Data Selection and Calculation of Micrometeorological Scales

Measurements during 23–27 May 2005 at the Dugway Proving Grounds (Utah; nominal coordinates of site—longitude 113°27.07′ W; latitude 40° 8.1′ N; elevation 1296 m above sea level) provided 32 one-hour daytime records of velocity from each of eight Campbell Scientific CSAT3 sonic anemometers (path length ≈0.12 m; sampled at 20 Hz). Four of these anemometers were located at height $z = 3$ m on an east–west transect at distances $y = (60, 50, 40, 30)$ m westward of a 26-m tower, while the other four sonic anemometers were at heights $z = (8.71, 12.52, 17.94, 25.69)$ m on that tower (although a further eight anemometers were operated, we excluded their signals to avoid sampling a region of the flow disturbed by downwind obstacles; see Wilson 2008, for further details). All anemometers were oriented for winds from the nominal north (azimuth angle $\beta = 0$), and we selected runs according to the following criteria: mean wind direction $|\overline{\beta}| \leq 30°$; friction velocity $u_* \geq 0.1$ m s^{-1}; Obukhov length $L < 0$; run start-time no sooner than 90 min after sunrise, run end-time no later than 60 min before sunset; and (where we give here any result stemming from the application of Taylor's frozen turbulence hypothesis) data were excluded from any anemometer at which the turbulence intensity $\sigma_u/\overline{u}$ (ratio of streamwise velocity standard deviation to the mean velocity) exceeded ½. Note that we did not assign individual values of (u_*, L) for each anemometer, but computed representative governing parameters for each run according to

$$u_*^4 = \left(\overline{\overline{u'w'}}\right)^2 + \left(\overline{\overline{v'w'}}\right)^2 , \tag{2}$$

$$T_* = -\,\overline{\overline{w'T'}}/u_* , \tag{3}$$

$$L = \frac{u_*^2\, T_0}{k_v\, g\, T_*} , \tag{4}$$

where $\overline{\overline{w'T'}}$ denotes the average value of the kinematic heat flux density $\overline{w'T'}$ over the four sonic anemometers on the transect, etc. Prior to the extraction of these statistics a double coordinate rotation, sequentially enforcing $\overline{v} = 0$ then $\overline{w} = 0$ (e.g. Wilczak et al. 2001), had

been performed individually for each anemometer, a step that was necessary because precise leveling of the higher sonic anemometers had not been possible.[5]

As with many previous authors, we inferred ϵ by fitting the Kolmogorov spectrum to the inertial subrange of streamwise spectra (details below), the approach recommended by Chamecki and Dias (2004) who considered that Albertson et al. (1997) had placed more confidence than warranted in the inference of ϵ from the third-order structure function. Before giving results we document the procedure used to compute spectra and deduce the dissipation rate.

2.2 Spectral Calculations

After the above-noted two-angle coordinate rotation to define 1-h time series of the streamwise component u', spectra were estimated using MATLAB's Fast Fourier Transform routine.[6] For each run (and each instrument) several estimates of the spectrum were computed from an $N = 2^{16}$ member series, each nominally covering one hour (true duration 54.61 min). In each case the "raw" spectrum was an unsmoothed periodogram (the 2^{16}-point time series had been tapered by application of a Hamming window, but the periodogram differed negligibly if this window was not applied). This spectrum being unsatisfactory for the estimation of ϵ, following Kaimal et al. (1972) we computed a smoothed spectrum separately over low and high frequency bands. For the low frequency band, a block-average time series was created by applying a 16-point block-average to the original time series (non-overlapping blocks) and the spectral estimate was computed after first applying a 4096-point Hamming window to the block-averaged series ("block-average spectrum"). For the high frequency band each original time series was divided into 16 non-overlapping consecutive blocks, each block containing 4096 points; a periodogram was computed for each block (after application of a 4096-point Hamming window) and the 16 spectra were averaged to produce the "composite spectrum." The low- and high-frequency spectral estimates, thus computed, overlap over two decades (0.005–0.625 Hz). A further spectral estimate ("Log av") was obtained by averaging the "raw" spectrum within each of fifty frequency bands, these spanning the frequency axis with equal intervals in $\log f$. Figure 1 illustrates the consistency of these several variants of the spectrum. At low frequency the "raw" spectrum is similar to (or coincides with) the "block-average" spectrum—the latter providing no spectral estimate at high frequency due to low-pass filtering. Conversely, due to its being based on a shorter record length the "composite spectrum" does not extend to low frequency.

A natural question is whether the Dugway spectra resemble "standard" surface-layer spectra?—there is no reason to expect they would not. In this context it is useful to appeal to the empirical spectral curve of Kaimal (1978), which specifies the spectrum for given $(u_*,\ L,\ \delta)$ where δ is the depth of the boundary layer (in the present case, δ was not measured). Conforming the Kaimal spectral curve to Dugway block-average spectra by least squares fitting (with δ treated as free to be optimized) we found that values thereby obtained for the ABL depth ("δ_K") were plausible, and that in many (though not all) cases the Dugway spectra

[5] Although it never exceeded 2°, the rotation angle $\overline{\alpha}$ required to yield $\overline{w} = 0$ was systematically largest for winds from the north, i.e. $|\overline{\beta}| \approx 0°$, winds that therefore were symmetrically incident on the frames of the sonic anemometers. All anemometers displayed a similar and *systematic* relationship between $\overline{\alpha}$ and the mean azimuth angle $\overline{\beta}$, on top of which was superposed a random variation. This consistent pattern is not attributable to a slope of the dry lake bed or anemometer tilt, and is presently under investigation.

[6] To check our application of the software, we computed the power spectrum of an artificial time series generated by a Markov chain, and compared this with the known (analytical) spectrum. The computed spectrum was correct, other than in regard to an aliasing error at the high frequency end, and irregularity at the low frequency end attributable to sampling error.

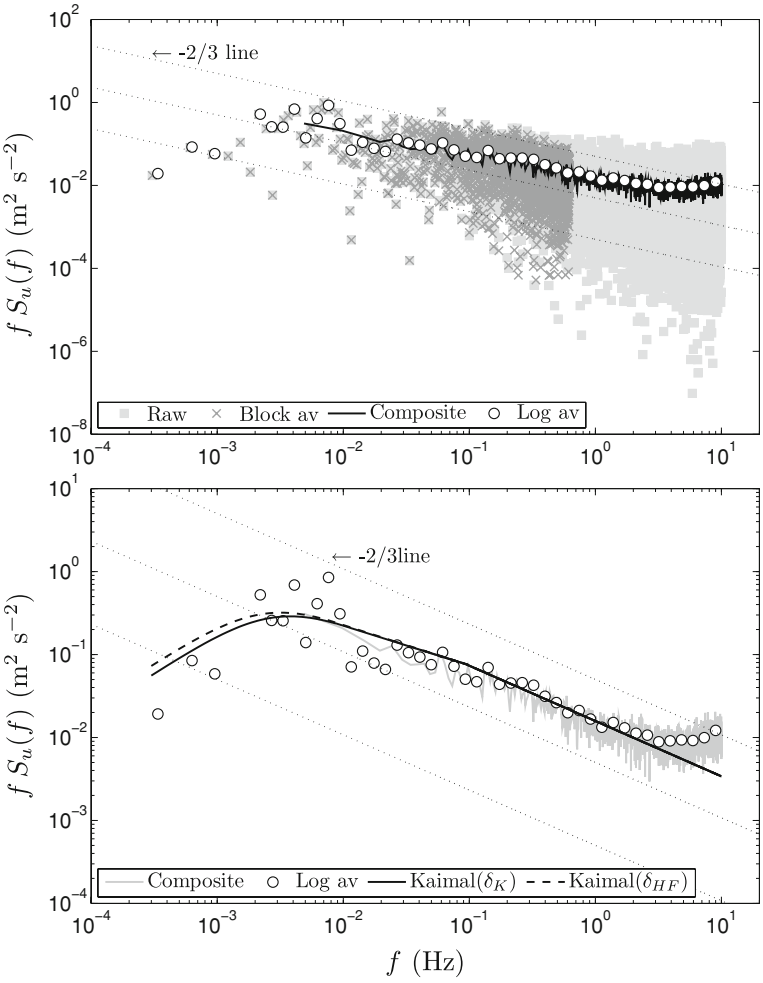

Fig. 1 An example of the Dugway velocity spectra: the computed u' spectrum (distinguishing the various estimates defined in Sect. 2.2) for the uppermost sonic anemometer on the tower ($z = 25.69$ m), for the hour centred on 1447 MDT (Mountain Daylight Time) 24 May, 2005. During this period $L = -4.0$ m (thus $z/L = -6.4$), $u_* = 0.22$ m s^{-1}, and mean horizontal wind speed at the sonic height was $\overline{u} = 4.99$ m s^{-1}. *Heavy solid and heavy dashed lines* on the lower panel are Kaimal's (1978) spectral curves for two values of the ABL depth: *solid line*, the value ($\delta_K = 850$ m) optimizing the fit of Kaimal's spectral curve to the block-averaged spectrum; and (*dashed line*) the value ($\delta_{HF} = 1008$ m) obtained from the surface heat flux and temperature trend (see Wilson 2008)

resembled the classic spectra. As an example the lower panel of Fig. 1 compares Kaimal's empirical spectrum with the computed spectrum.

To give a more comprehensive summary of the Dugway u' spectra we present in Fig. 2 the computed spectra at the transect height (3 m) for each of the 32 runs; each spectrum plotted is the average of four computed spectra, i.e. one per sonic anemometer on the transect (restricting to the 3-m sonics provides smoother spectra, but reduces the $-z/L$ range represented by the factor 26/3, the height ratio of the uppermost sonic and the transect). The spectra shown on Fig. 2 stem from the "Log av" method, and in order to collapse the spectra in the inertial

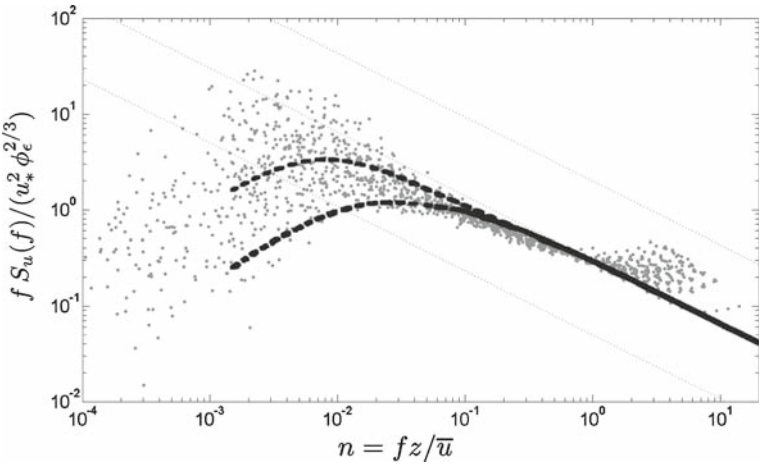

Fig. 2 Power spectra $S_u(f)$ at $z = 3$ m for all 32 runs, each being the average of the four spectra provided by the four anemometers on the transect. The *dashed lines* are taken from Kaimal et al. (1972; Fig. 5), and give the upper and lower limits of the band covered by the Kansas spectra for unstable stratification ($-2 \le z/L \le 0^-$). Normalization has collapsed the Dugway spectra in the inertial subrange, but spreads the signature of aliasing along the $fz/\overline{u}$ axis

subrange we have scaled as $fS(f)u_*^{-2}\phi_\epsilon^{-2/3}$ versus $fz/\overline{u}$, f being the natural frequency. Superposed are lines (from Kaimal et al. 1972, Fig. 5) that bound the shaded region representing the ensemble of Kansas spectra covering the range $-2 \le z/L \le 0^-$. Several points need to be made in regard to Fig. 2. Firstly, the Dugway spectra do (as expected) collapse in the inertial subrange, although the high frequency upturn due to aliasing, appearing at different $fz/\overline{u}$ in runs with different $\overline{u}$, distorts the spectra at the highest computed frequencies. Secondly we note that the dashed line giving the lower limit for normalized spectral density in the energy-containing range of unstable Kansas spectra, delineates the lower limit for the Dugway spectra quite effectively. Thirdly, however, the upper dashed line does not "contain" the Dugway spectra, which in many cases show higher spectral density in that range. Recall that with increasing $\delta/|L|$ it is expected there will be more power in the energy-containing range, and that the Kansas data were not selected or classified in terms of that ratio (which had not been measured). In summary then, the Dugway u' spectra are consistent with those of the Kansas experiment.

2.3 Extraction of ϵ from the Composite Spectrum

If Taylor's frozen turbulence hypothesis is used to transform Kolmogorov's wavenumber ($\kappa = 2\pi f/\overline{u}$) spectrum for the inertial subrange into frequency (f) space, one has

$$f\,S_u(f) = T_{11}\,\alpha_u\,\epsilon^{2/3}\left(\frac{2\,\pi\,f}{\overline{u}}\right)^{-2/3}, \tag{5}$$

where the factor T_{11} is defined by

$$T_{11} = 1 - \frac{\overline{u'^2}}{9\,\overline{u}^2} + \frac{2\,\overline{v'^2}}{3\,\overline{u}^2} + \frac{2\,\overline{w'^2}}{3\,\overline{u}^2} \tag{6}$$

and was introduced by Wyngaard and Clifford (1977) as an (approximate) correction for variability in the speed of convection of small eddies past the sensor. In the majority of cases T_{11} was not very different from unity, and we will show inferred values of ϵ both with and without this correction. Re-arranging Eq. 5, the TKE dissipation rate can be expressed as

$$\epsilon = \frac{2\pi}{\overline{u}} \left[\frac{f^{5/3} S_u(f)}{T_{11}\, \alpha_u} \right]^{3/2}. \tag{7}$$

Spectral density at frequency $f = 1$ Hz for substitution into Eq. 7 was evaluated from the equation for a straight line with prescribed slope $(-2/3)$ relating $\log[f\, S_u(f)]$ to $\log f$, best fitted to the inertial subrange region of the composite spectra—more specifically, in the range $\overline{u}/(2z) \le f \le 2$ Hz, where the lower frequency limit is that given by Eq. 12 of Kaimal (1978). Following Sreenivasan (1995) (see also Pope 2000, Eq. 6.242) we assumed $\alpha_u = 0.5$, although the resulting estimates of ϵ must be regarded as carrying an uncertainty of order 10% (at a minimum), for the Kansas experiments gave $\alpha_u = 0.52 \pm 0.04$ (Wyngaard and Coté 1971, Fig. 6), while Oncley et al. (1996) found $\alpha_u = 0.54 \pm 0.03$ (see also Table 1 of Hogstrom 1990).

3 Results

Recall that the (normalized) turbulent kinetic energy budget for a stationary and horizontally-uniform ASL reads

$$0 = \phi_m - z/L - \phi_t - \phi_p - \phi_\epsilon \tag{8}$$

(here we follow the sign convention of Kaimal and Finnigan 1994), where from left-to-right the terms are respectively shear production $P_S = \phi_m$, buoyant production $P_B = -z/L$, turbulent transport, pressure transport, and viscous dissipation. Figure 3 shows that the Dugway data organize tidily as a function of z/L, and that over the entire range of unstable stratification[7]

$$\phi_\epsilon \approx \phi_m - z/L, \tag{9}$$

as if the sum of turbulence and pressure transport in Eq. 8 were negligible. This was unexpected, since it is not generally considered the unstable surface layer is in local equilibrium (e.g. Kaimal and Finnigan 1994). In any case the assumption of local equilibrium (Eq. 9) certainly provides a superior fit to the data than does Eq. 1 or the slight revision of it suggested by Kaimal (1978) and Caughey and Wyngaard (1979).

Following the 'directional dimensional analysis' of some earlier authors (especially Kader 1992), Albertson et al. (1997) broke the continuous $z/|L|$ axis of Monin–Obukhov similarity theory into three non-overlapping bands or regions, their dynamic sublayer $(-z/L < 0.04)$ representing the regime where buoyant production is of negligible importance (flux Richardson number R_i^f asymptotically zero), their free convection sublayer $(-z/L > 2)$ representing the opposite asymptotic regime $(|R_i^f| \sim \infty)$, and their dynamic-convective sublayer $(0.12 \le -z/L \le 1.2)$ being (ostensibly) a categorically more complex regime owing (in part) to the action of the redistribution terms in the budgets of $(\overline{u'^2}, \overline{v'^2}, \overline{w'^2})$. The

[7] We have shown $\phi_\epsilon(z/L)$ with the dimensionless wind shear evaluated as $\phi_m = (1 - 28z/L)^{-1/4}$ (Dyer and Bradley 1982), although the curve is almost indistinguishable if one instead uses $\phi_m = (1 - 16z/L)^{-1/3}$ (e.g. Frenzen and Vogel 2001).

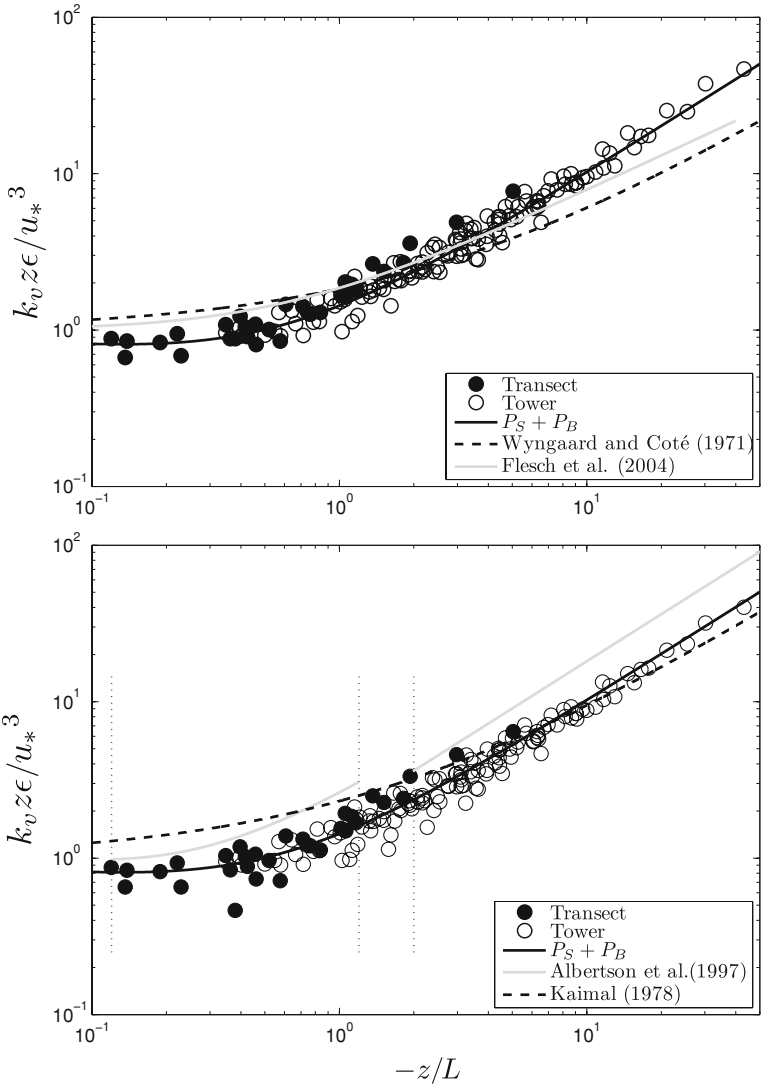

Fig. 3 Normalized TKE dissipation rate for unstable Dugway runs. Values on lower panel derive from spectral densities that were multiplied by the Wyngaard–Clifford correction factor T_{11}, whereas values shown on upper panel are from uncorrected spectra (the curve $P_S + P_B$ of the normalized TKE production rate is shown on both panels, providing a basis to judge the importance of the T_{11} correction). *Solid symbols* hold greater significance than *open symbols*, for they derive from the average of four spectra at $z = 3$ m on the transect whereas each *open symbol* derives from a single instrument (and run). *Dotted vertical lines* on lower panel demarcate the $-z/L$ boundaries of the dynamic-convective sublayer and the free convection sublayer, and highlight the discontinuity of a parametrization suggested by Albertson et al. (1997). Details of other curves are given in the text

data of Fig. 3 do not suggest the need for this fragmentation of the z/L axis, and while they do not adequately cover the region designated 'dynamic sublayer,' neither do they appear conclusively *incompatible* with $\phi_\epsilon = 1$ in the neutral limit.

The Dugway measurements permit evaluation of

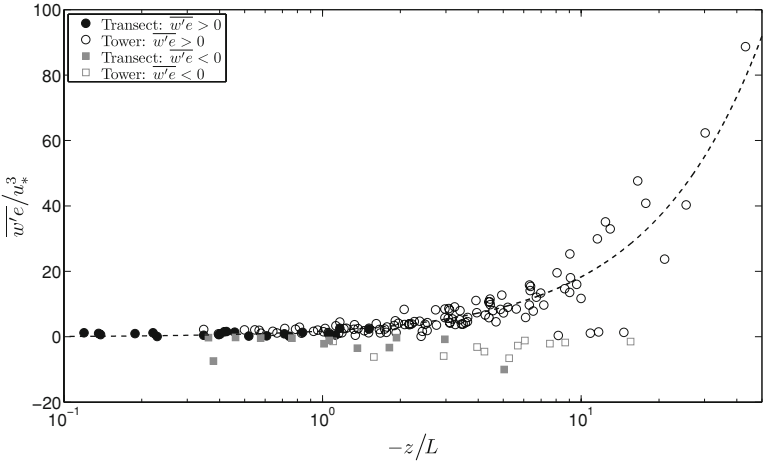

Fig. 4 Normalized vertical flux of TKE versus $-z/L$. Again, *solid symbols* are the average across the four sonics on the transect at $z = 3$ m and deserve more weight than *open symbols*, while *square symbols* have been used to distinguish negative values of $\overline{w'e}$. Where the derivative of the TKE flux vanishes, the turbulent transport term ϕ_t in the TKE budget also vanishes. The *dashed line* corresponds to $\phi_t(z/L) = -0.74\, z/L$, which emerged from a linear regression of $\overline{w'e}/u_*^3$ against $-z/L$ with all negative values of $\overline{w'e}$ having been ignored

$$\phi_t\left(\frac{z}{L}\right) \equiv \frac{k_v z}{u_*^3}\,\frac{\partial\ \overline{w'(u'_j u'_j)/2}}{\partial z} = k_v\,\frac{\partial\ \overline{w'e}/u_*^3}{\partial\ \ln z} = k_v\,\frac{\partial\ \overline{w'e}/u_*^3}{\partial\ \ln z/|L|} \tag{10}$$

where $e \equiv (u'_j u'_j)/2$ is a notational shorthand, and (since in any one run L is a constant) $d \ln z/|L| \equiv d \ln z$. Figure 4, a plot of $\overline{w'e}/u_*^3$ versus $\ln(-z/L)$, strongly suggests that in the neutral limit ($z/|L| \to 0$) turbulent transport vanishes, while during unstable conditions TKE is exported to higher elevations (as in the Kansas data; see also Fig. 4 of Bradley et al. (1981), whose q^2 is equivalent to $q^2 = e$). The slope of a line of best fit to the scatter plot of $\overline{w'e}/u_*^3$ versus z/L (not shown) gave the result that $\phi_t(z/L) = -0.74\, z/L$ (fraction of variance explained $R^2 = 0.84$), which is broadly consistent with the earlier findings of Wyngaard and Coté (1971) and Caughey and Wyngaard (1979), and very close to the result of Frenzen and Vogel (2001). Please note that to compute this result for ϕ_t, which in conjunction with Eq. 9 implies $\phi_p(z/L) \approx +0.74\, z/L$, we ignored three runs that had produced most of the small negative values of $\overline{w'e}$ seen on Fig. 4; had those three runs been included, then $\phi_t = -0.70\, z/L$ with $R^2 = 0.69$. There was no obvious association of negative $\overline{w'e}$ with extreme values of the scaling parameters (u_*, L, δ), but we nonetheless felt justified in neglecting them, in part because for those three runs values of $\overline{w'e}$ differed very notably from one to another of the four sonic anemometers on the transect, and in part because Wyngaard and Coté (1971) remarked of the Kansas data that "The turbulent energy flux (i.e. our $\overline{w'e}$) was positive in every unstable case."

4 Conclusion

The balance of TKE production and dissipation rates reported above has to be interpreted as being *approximate*. As noted earlier the Kolmogorov coefficient α_u has been the subject

of much study in its own right, but a fractional uncertainty of order 10% is probably a fair assessment (see Hogstrom 1990), and implies a corresponding fractional uncertainty in ϵ (as derived here) of no less than 15%. Where earlier authors have reported the *absence* of local equilibrium, the imbalance has generally been of only this same order (e.g. Garratt 1972; McBean and Elliot 1975; Bradley et al. 1981; and later results summarized by Li et al. 2008, Table 2).

As usual, uncertainty surrounds the role of unmeasured pressure transport of TKE. The indication (Fig. 4) that turbulent transport vanishes in the limit $z/|L| \to 0$ does not prove that local equilibrium *must* prevail in the neutral ASL; and conversely, the fact that $\phi_t \neq 0$ in the unstable ASL does not forbid the possibility of local equilibrium—which could only happen, however, if the pressure and turbulent transport happened to cancel (as has been suggested to be the case by the measurements of McBean and Elliot 1975). All that can be said with certainty of the present results is that, across the entire range of $z/|L|$ sampled, Eq. 9, equivalent to the assumption of local equilibrium, provides a good approximation to the TKE dissipation rate—though no convincing justification can be given as to why that should be the case. On the strength of this finding (and see also footnote 4) it appears defensible to continue the practise (e.g. Wilson 2004, Sec. 2i) of specifying the coefficients of turbulence closure models to require local balance of TKE production and dissipation rates for the reference case of a neutral and horizontally-homogeneous surface layer.

There is also a direct practical utility to an improved parametrization of TKE dissipation rate, in that ϵ plays a central role in modern Lagrangian stochastic (LS) models of turbulent trajectories (Thomson 1987), in which context it can be related

$$C_0\,\epsilon = \frac{2\,\sigma_w^2}{\tau_L} \tag{11}$$

to a parameter τ_L that, loosely interpreted, amounts to the Lagrangian velocity decorrelation time scale (C_0 is a universal Kolmogorov constant). Flesch et al. (2004) documented a tracer gas experiment testing the performance of a backward LS model in the context of "inverse dispersion," i.e. the inference of an unknown gas emission rate Q by combining a measured downwind (mean) concentration C with a "backward" model of fluid element trajectories in the given (measured) micrometeorological conditions (the "bLS" method). The ϵ parametrization used in the bLS model (Eq. A13, Flesch et al. 2004) is plotted on Fig. 3 (it had stemmed originally from an optimization of the model fit to a small number of the classic Project Prairie Grass dispersion trials, by tuning the $\tau_L(z/L)$ profile). As noted by Flesch et al. (2004) this parametrization resembles Eq. 1, and therefore it does not fit the present (Dugway) data very well. When a subset ($N = 20$ cases of very unstable stratification, $-5\,\mathrm{m} \leq L \leq 0$) of the trials reported by Flesch et al. were re-analysed using Eq. 9 to specify $\epsilon(z/L)$, the mean value of the ratio Q_{bLS}/Q (of inferred to true source strength) improved from 1.42 to 1.22 (source strength less seriously overestimated), while the corresponding standard deviation (of the Q_{bLS}/Q ratio) was reduced from 0.89 to 0.39 (T.K. Flesch, personal communication, 2009).

Acknowledgements The sonic anemometer array was planned and operated by K. McNaughton, R. Clement, and J. Moncrieff (U. Edinburgh), with invaluable assistance from E. Swiatek and the late B. Tanner (Campbell Scientific Inc.). We are also grateful to D. Storwold and J. Bowers (U.S. Army Dugway Proving Ground) for infrastructure and support on site; and to J. Klewicki (U. Utah), who coordinated the efforts of a large team comprising individuals (and pooled equipment) from the University of Utah, University of Edinburgh, University of Minnesota, University of Melbourne, Imperial College, London, and the University of Alberta. The authors thank the unknown reviewers, and acknowledge financial support from the Natural Sciences and Engineering Research Council of Canada.

References

Albertson J, Parlange M, Kiely G, Eichinger W (1997) The average dissipation rate of turbulent kinetic energy in the neutral and unstable atmospheric surface layer. J Geophys Res 102:13423–13432

Bradley EF, Antonia RA, Chambers AJ (1981) Turbulence Reynolds number and the turbulent kinetic energy balance in the atmospheric surface layer. Boundary-Layer Meteorol 21:183–197

Bradshaw P (1967) The turbulence structure of equilibrium boundary layers. J Fluid Mech 29:625–645

Bradshaw P (1978) Introduction. In: Topics in applied physics, Chapt. 1, pp. 1–44. Springer-Verlag, Berlin, 339 pp

Bradshaw P, Ferriss D, Atwell N (1967) Calculation of boundary-layer development using the turbulent energy equation. J Fluid Mech 28:593–616

Caughey S, Wyngaard J (1979) The turbulence kinetic energy budget in convective conditions. Q J Roy Meteorol Soc 105:231–239

Chamecki M, Dias N (2004) The local isotropy hypothesis and the turbulent kinetic energy dissipation rate in the atmospheric surface layer. Q J Roy Meteorol Soc 130:2733–2752

Dyer A, Bradley E (1982) An alternative analysis of flux-gradient relationships at the 1976 ITCE. Boundary-Layer Meteorol 22:3–19

Flesch T, Wilson J, Harper L, Crenna B, Sharpe R (2004) Deducing ground-air emissions from observed trace gas concentrations: a field trial. J Appl Meteorol 43:487–502

Frenzen P, Vogel C (1992) The turbulent kinetic energy budget in the atmospheric surface layer: a review and an experimental reexamination in the field. Boundary-Layer Meteorol 60:49–76

Frenzen P, Vogel C (2001) Further studies of atmospheric turbulence in layers near the surface: scaling the TKE budget above the roughness sublayer. Boundary-Layer Meteorol 99:173–206

Garratt J (1972) Studies of turbulence in the surface layer over water (Lough Neagh) Part II. Production and dissipation of velocity and temperature fluctuations. Q J Roy Meteorol Soc 98:642–657

Hanjalic K, Launder B (1972) A Reynolds stress model of turbulence and its application to thin shear flows. J Fluid Mech 52:609–638

Hogstrom U (1990) Analysis of turbulence structure in the surface layer with a modified similarity formulation for near neutral conditions. J Atmos Sci 47:1949–1972

Kader B (1992) Determination of turbulent momentum and heat fluxes by spectral methods. Boundary-Layer Meteorol 61:323–347

Kaimal J (1978) Horizontal velocity spectra in an unstable surface layer. J Atmos Sci 35:18–24

Kaimal J, Finnigan J (1994) Atmospheric boundary layer flows. Oxford University Press, Oxford, 289 pp

Kaimal J, Wyngaard J, Izumi Y, Cote O (1972) Spectral characteristics of surface-layer turbulence. Q J Roy Meteorol Soc 98:563–589

Launder BE, Spalding DB (1974) The numerical computation of turbulent flows. Comp Meth Appl Mech Eng 3:269–289

Li X, Zimmerman N, Princevac M (2008) Local imbalance of turbulent kinetic energy in the surface layer. Boundary-Layer Meteorol 129:115–136

McBean G, Elliot J (1975) The vertical transport of kinetic energy by turbulence and pressure in the boundary layer. J Atmos Sci 32:753–766

Metzger M, Holmes H (2008) Time scales in the unstable atmospheric surface layer. Boundary-Layer Meteorol 126:29–50

Oncley S, Friehe C, Larue J, Businger J, Itsweire E, Chang S (1996) Surface-layer fluxes, profiles, and turbulence measurements over uniform terrain under near-neutral conditions. J Atmos Sci 53:1029–1044

Pope S (2000) Turbulent flows. Cambridge University Press, Cambridge, 771 pp

Raupach M, Antonia R, Rajagopalan S (1991) Rough-wall turbulent boundary layers. Appl Mech Rev 44:1–25

Richardson L (1920) The supply of energy from and to atmospheric Eddies. Proc R Soc Lond Ser A 97: 354–373

Sreenivasan K (1995) On the universality of the Kolmogorov constant. Phys Fluids 7:2778–2784

Tennekes H, Lumley J (1972) A first course in turbulence. MIT Press, Cambridge, 300 pp

Thomson D (1987) Criteria for the selection of stochastic models of particle trajectories in turbulent flows. J Fluid Mech 180:529–556

Townsend A (1961) Equilibrium layers and wall turbulence. J Fluid Mech 11:97–120

Townsend A (1976) The structure of turbulent shear flow, 2nd edn. Cambridge University Press, Cambridge, 440 pp

Wilczak J, Oncley S, Stage S (2001) Sonic anemometer tilt correction algorithms. Boundary-Layer Meteorol 99:127–150

Wilson J (2004) Oblique, stratified winds about a Shelter Fence, II: comparison of measurements with numerical models. J Appl Meteorol 43:1392–1409

Wilson J (2008) Monin–Obukhov functions for standard deviations of velocity. Boundary-Layer Meteorol 129:353–369

Wyngaard J, Clifford S (1977) Taylor's hypothesis and high-frequency turbulence spectra. J Atmos Sci 34: 922–929

Wyngaard J, Coté O (1971) The budgets of turbulent kinetic energy and temperature variance in the atmospheric surface layer. J Atmos Sci 28:190–201

Wyngaard J, Cote O, Rao K (1974) Modeling the atmospheric boundary layer. Adv Geophys 18A:193–212